Journal of Energy Challenges and Mechanics
http://www.nscj.co.uk/JECM/

ISSN 2056-9386
Volume 3 (2016) issue 3, article 6

Study on the Gear Ratio for a Tidal Current Power Generation System using the Constant Turbine Output Control Method

使用恒定涡轮输出控制方法的潮汐流发电系统之齿轮比研究

Kentaro Tsuji[1*], Kazuhisa Naoi[1], Mitsuhiro Shiono[1]

[1] *Department of Electrical Engineering, College of Science and Technology, Nihon University, Chiyoda-ku, Tokyo 101-8308, Japan*

tsuji.kentaro@nihon-u.ac.jp

Accepted for publication on 14th September 2016

Abstract - **Tidal current is the flow of sea water due to the tidal phenomenon. Therefore, it is possible to predict power output of the tidal current power generation system, which is more advantageous than other renewable energy sources, when the tidal current power generation system is connected to the power grid and operated.**

Power generation method of tidal current power generation systems is a fixed-speed method or a variable-speed method. The authors have examined the gear ratio and generator capacity of the tidal current power generation system using the maximum power point tracking (MPPT) control scheme. The capacity factor of the system which influences cost of power generation was about 14%. To increase the capacity factor of tidal current power generation systems, we propose the tidal current power generation system which can be controlled to constant turbine output and we examined a method of deciding the gear ratio and generator capacity which maximize generated energy.

First, this paper examines the speed control model which is operated using the constant turbine-output control scheme. The target value of the speed control model is rotational speed of generator for each current speed. Second, this paper examines the gear ratio and generator capacity which maximize generated energy, when the tidal current power generation system is operated using constant turbine-output control scheme.

This paper shows that the constant turbine-output control scheme increases generated energy, capacity factor and energy conversion efficiency in comparison with the MPPT control scheme. On the other hand, the constant turbine-output control scheme decreases generator capacity in comparison with the MPPT control scheme. The results of the speed control model using calculated the gear ratio and generator capacity show a good dynamic response to variation of current speed.

Keywords - **tidal current power generation, Darrieus type water turbine, DFIG, constant turbine-output control method, gear ratio**

I. INTRODUCTION

Methods for generating electricity from renewable energy sources are of growing interest for achieving a stable energy supply and as countermeasures against global warning. One form of renewable energy is tidal currents, flows of sea water caused by the rise and fall of the tide. The direction of these flows reverses every half-period; the length of the period varies with location, and is either about half a day or a full day [1]. Thus, tidal current power generation offers advantages in terms of connecting to a power grid, as the power output is predictable and little influenced by the weather.

The authors have investigated a Darrieus turbine-based tidal current power generation system whose generator transforms the rotational energy of the turbine into electrical energy. We have conducted water channel tests and open water tests of the characteristics of a Darrieus-type water turbine and of the electric power it can generate [2][3], in preparation for use of this turbine in a tidal current power generation system.

The power input to a tidal current power generation system varies in a similar way to a wind power generation system. Power generation method of tidal current power generation

systems is a fixed-speed method or a variable-speed method. Variable-speed methods have received the most attention, as they are more efficient in converting tidal current energy to electrical energy. Two types of generators are used in variable-speed methods, doubly fed induction generators (DFIGs) and synchronous generators. In a DFIG-based system, an inverter is placed between the rotor circuit of the generator and the power grid; this has the advantage of allowing the inverter to be of lower capacity than that for a synchronous generator [4]. Thus, the tidal current power generation system we have investigated employs a variable-speed DFIG.

As mentioned above, in the field of wind power generation, there have been investigations of systems incorporating DFIGs [5][6] and models of speed controls for generators [7-9], just as in the case of tidal current power generation. However, those investigations all examined systems in which the gear ratio, the generator capacity, or both, were fixed. The present investigation addressed gear ratios and generator capacities for tidal current power generation systems to maximize the generated energy without overloading it. One of our previous investigations revealed that the annual capacity factor of this system was about 14% while operated with maximum power-point tracking (MPPT) [10]. For comparison, figures of 12% and 20% are commonly quoted for solar and wind power generation systems, respectively [11]; thus, this annual capacity factor exceeds that for solar power generation systems.

Nonetheless, when operating with MPPT, the generator must be large enough to accommodate the maximum current speed occurring during the year, and this detracts from economic efficiency. We propose reducing the generator capacity and, in order to further improve the annual capacity factor of this tidal current power generation system, to implement a constant turbine-output control scheme. The objective of this study was to identify the optimal gear ratio and the generator capacity providing the maximum generated energy without overloading the generator while the tidal current power generation system is operated under this control scheme.

This study is presented as follows: First, a method of approximating the characteristics of the water turbine and a probability density function for the occurrence of current speeds are described. Then, a model of the speed controller for the tidal current power generation system is examined. A procedure is investigated for identifying the gear ratio and the generator capacity that will allow maximizing the generated energy without overloading the generator while the tidal current power generation system is operated under this control scheme. Finally, the response of a system incorporating the identified gear ratio and generator capacity operating in currents of varying speeds is examined.

II. Tidal Current Power Generation System Based on Darrieus Water Turbine

2.1. Power Output Characteristics of Darrieus Water Turbine

We have developed and conducted experiments in a water channel and in the ocean with a tidal current power generation system based on a Darrieus water turbine [2][3]. This turbine contained straight blades, and is referred to as a "straight-bladed vertical-axis water turbine" (Fig. 1(a)). The profile for these blades was based on the symmetric

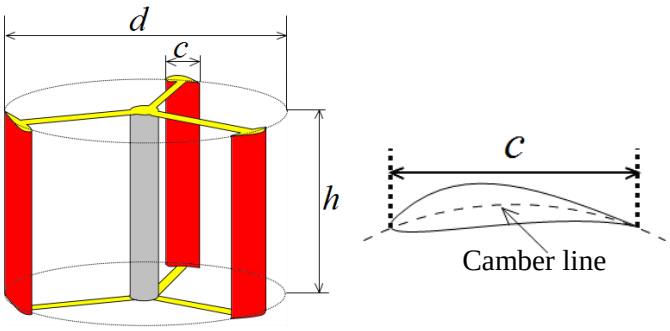

(a) Turbine configuration (b) Shape of blade

Fig. 1, Schematic diagram of Darrieus water turbine.

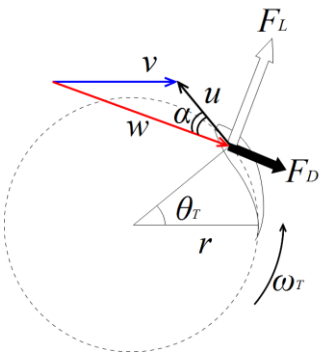

Fig. 2, Forces exerted by flow.

NACA63$_3$-018 [12], but on a camber line fitting the blade path (Fig. 1(b)). The blades were placed at uniform intervals around the circumference of the turbine.

We first describe the operating principles of the Darrieus water turbine. We begin with a simple 2-dimensional view of the plane of rotation in Fig. 1(a). A single blade rotates with a circumferential speed u about a blade path of radius r at an angle θ_T in a flow field moving at velocity v. Figure 2 shows the relation between u and v. The relative flow (relative velocity) w at the blade is given by the vector sum of v and u:

$$w = v\sqrt{1+2\lambda\cos\theta_T+\lambda^2} \tag{1}$$

where λ is the tip speed ratio (= u/v = $r\omega_T/v$), r is the turbine radius, ω_T is the angular speed of the turbine.

When the fluid strikes the blade, it exerts a force against it. This force can be resolved into two components, the drag force F_D acting in the same direction as the relative fluid velocity, and the lift force F_L acting in a direction perpendicular to F_D. These forces are given by Eqs. (2) and (3), using the fluid density ρ and blade area A.

$$F_L = \frac{1}{2} C_L \rho A w^2 \tag{2}$$

$$F_D = \frac{1}{2} C_D \rho A w^2 \tag{3}$$

C_L and C_D are the coefficients of lift and of drag, respectively, and are influenced by many factors including the blade profile, angle of attack, Reynolds number, and blade surface roughness. α is the angle of attack and is given by Eq. (4) on the basis of Fig. 2.

$$\alpha = \tan^{-1}\left(\frac{\cos\theta_T}{\sin\theta_T + \lambda} \right) \tag{4}$$

The torque T_1 arising in a single blade is given by:

$$T_1 = \frac{1}{2} \rho r A w^2 \left(C_L \sin\alpha - C_D \cos\alpha \right) \tag{5}$$

The mean torque T_q generated by n blades during a single revolution of the turbine is then:

$$T_q = \frac{n}{2\pi} \int_0^{2\pi} T_1 d\theta_T \tag{6}$$

The dimensionless torque coefficient C_T in Eq. (7) is introduced to evaluate the torque:

$$C_T = \frac{T_q}{0.5 \rho S r v^2} \tag{7}$$

where S (=d×h) is the swept area of the water turbine, d is the turbine diameter, and h is the blade height. The turbine output power P_{To} is estimated using:

$$P_{To} = \omega_T T_q \tag{8}$$

If the input fluid power over the swept turbine area S is P_{Ti}, this is given by:

$$P_{Ti} = \frac{1}{2} \rho S v^3 \tag{9}$$

The water turbine efficiency, i.e., its power efficiency C_P, is expressed as

$$C_P = \frac{P_{To}}{P_{Ti}} \tag{10}$$

2.2. Approximation of Water Turbine Characteristics with a Spline Function

We now consider the method for approximating the water turbine characteristics, which will be needed in order to calculate the generated energy and to examine the turbine speed control model. These characteristics are approximated using a (2m–1)-dimensional spline smoothing function. The turbine characteristics obtained from the water channel tests were the turbine speed and the torque [3]; in this study, the torque coefficient C_T is approximated with a spline smoothing function.

The smooth curve close to the data points obtained in the experiment is designated $f_s(x)$, the coordinate system of the obtained data is (x_1,y_1), (x_2,y_2), …, (x_n,y_n), and ε defined in Eq. (11) is employed as the evaluation indicator showing how faithfully and smoothly $f_s(x)$ reproduces the data points.

$$\varepsilon = \sum_{i=1}^{n} w_i \left\{ f_s(x_i) - y_i \right\}^2 + g \int_{x_1}^{x_n} \left\{ f_s^{(m)}(x) \right\}^2 dx \tag{11}$$

Here, $f_s^{(m)}(x)$ is the m^{th} derivative of $f_s(x)$, and w_i and g are weighting coefficients with values $0 < w_i \leq 1$ and $g > 0$. The first term in this index denotes how faithfully $f_s(x)$ reproduces the data points. The second term indicates how smooth $f_s(x)$ is. Thus, when ε has been minimized, $f_s(x)$ has reached its smoothest possible shape under coefficient g. The (2m-1)-dimensional spline smoothing function is given by:

$$f_s(x) = p_{m-1}(x) + \sum_{i=1}^{n} c_i \left(x - x_i \right)_+^{2m-1} \tag{12}$$

Here, $\left(x - x_i \right)_+^{2m-1}$ is the $(2m\text{-}1)^{\text{th}}$ truncated power function and $p_{m-1}(x)$ is a $(m\text{-}1)^{\text{th}}$ polynomial given by

$$p_{m-1}(x) = \sum_{i=0}^{m-1} b_i x^i \tag{13}$$

The c_i in Eq. (12) are constants satisfying m conditions given by

$$\sum_{i=1}^{n} c_i x_i^{\,k} = 0 \quad (k=0, 1, 2, \ldots, m\text{-}1) \tag{14}$$

It has been shown [13] that Eq. (11) is a function minimizing ε when the n conditions in Eq. (15) are satisfied by the spline smoothing function $f_s(x)$ in Eq. (12).

$$f_s(x_j) + (-1)^m \cdot g \cdot (2m-1)! c_j w_j^{-1} = y_j \ (j=1, 2, \ldots, n) \tag{15}$$

Table 1 presents the specifications of the water turbine constructed for water channel experiments, in which the turbine characteristics were identified. Using w_i=1 in Eq. (11), g was varied until a minimum value for ε was found; this is shown in Table 2. Here, ε_w represents the first term and ε_g represents the 2nd term in Eq. (11). The value for g in Table 2 was employed to approximate C_T, and the results are shown in Fig. 3. C_T is described by the following cubic (m=2) spline smoothing function:

$$C_T = d_0 + d_1 \lambda + d_2 \lambda^2 + d_3 \lambda^3 \tag{16}$$

Here, $d_0 - d_3$ are constants which differ in every sector of the approximated data. C_P is a function of λ and C_T, (Eq. (17)) and is shown in Fig. 4:

$$C_P = \lambda C_T \tag{17}$$

TABLE 1, Specifications of Tested Water Turbine

Number of blades n	3
Diameter d [mm]	300
Height h [mm]	200
Chord length c [mm]	55.3
Solidity σ	0.176

TABLE 2, MINIMUM VALUES OF ε AND g FOR DIFFERENT CURRENT SPEEDS

Current speed v [m/s]	Weighting factor g	Evaluation index ε	ε_w	ε_g
1.0	2.7×10^{-2}	2.6×10^{-2}	2.8×10^{-4}	2.6×10^{-2}
1.2	3.1×10^{-2}	2.2×10^{-2}	2.6×10^{-4}	2.2×10^{-2}
1.4	3.9×10^{-2}	2.9×10^{-2}	4.5×10^{-4}	2.8×10^{-2}

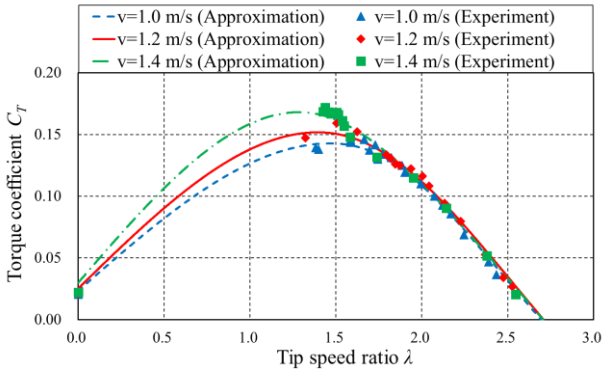

Fig. 3, Approximation of C_T characteristics using spline.

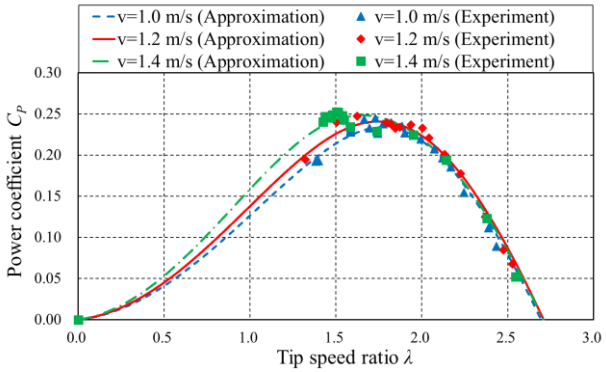

Fig. 4, Approximation of C_P characteristics using spline.

From Table 2, the data are most closely and smoothly approximated when ε is minimized; ε is lowest at a current speed of v = 1.2 m/s. Thus, the investigation in this study was carried out using the approximation curve for v = 1.2 m/s.

2.3. PROBABILITY DENSITY FUNCTION FOR OCCURRENCE OF CURRENT SPEEDS

Generally, the direction and speed of tidal currents change every 6 hours. The estimated values for current speed near the center of Akashi Strait [14] provided by the Japan Coast Guard Hydrographic and Oceanographic Department from January to December in 2003 and 2004 were used as data samples. Figure 5 presents those speed data.

We created a histogram as a representative probability distribution of these speeds v_j. A linear interpolation was performed to find the times t_j, t_{j+1} at which speeds v_j, v_{j+1} occur. This procedure was carried out throughout the observation time T. A Darrieus turbine rotates in the same direction, regardless of the direction of the incoming flow, so only the absolute value (i.e., speed). The symbols denoting absolute values will be omitted below. The probability of occurrence of a v value between v_j and v_{j+1} during time T is given by:

$$F(v_j \le v \le v_{j+1}) = \frac{\sum \Delta T_j}{T} \tag{18}$$

where $\Delta T_j = t_{j+1} - t_j$ and $\Sigma \Delta T_j$ is the sum of the time intervals when speeds between v_j and v_{j+1} occurred.

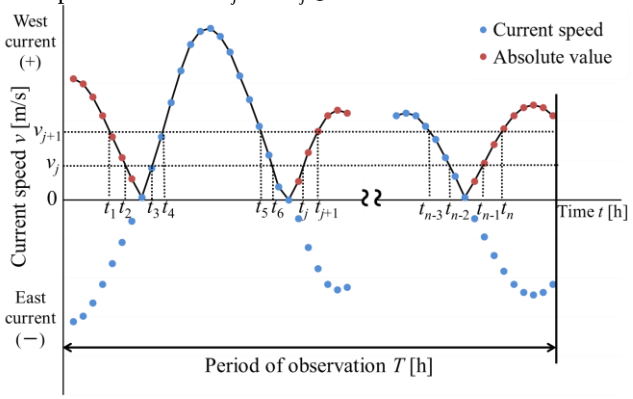

Fig. 5, Examples of tidal current speed.

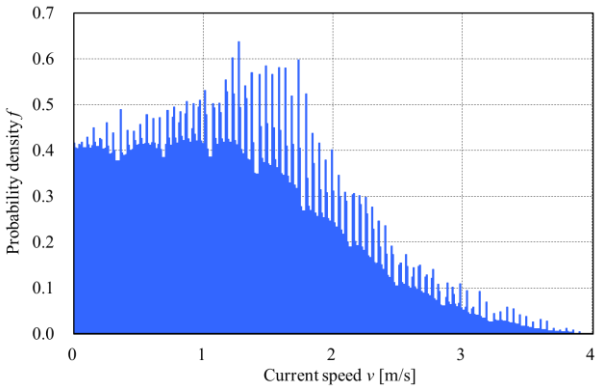

Fig. 6, Probability density function for current speed (2003).

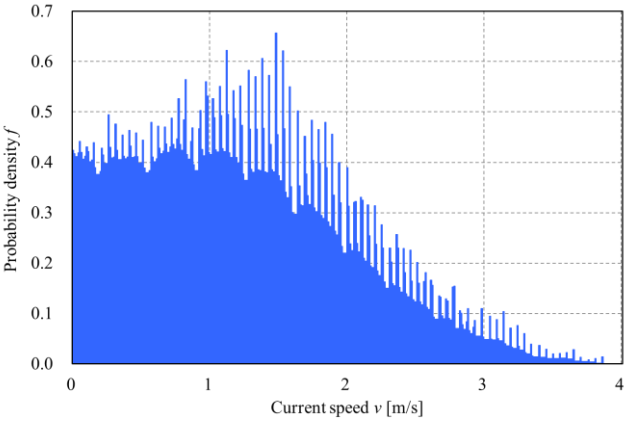

Fig. 7, Probability density function for current speed (2004).

The probability density function for the current speed is written as:

$$f(v) = \frac{F(v_j \le v \le v_{j+1})}{\Delta v} \tag{19}$$

where $0 \le v \le v_m$ and $\Delta v = v_{j+1} - v_j$. v_m is the maximum current speed during time T. Figures 6 and 7 show $f(v)$ for the years 2003 and 2004, respectively, where Δv was 0.01 m/s.

2.4. DFIG-BASED TIDAL CURRENT POWER GENERATION SYSTEM

Figure 8 shows a schematic illustration of the tidal current power generation system incorporating a DFIG. Here, P_{To} is

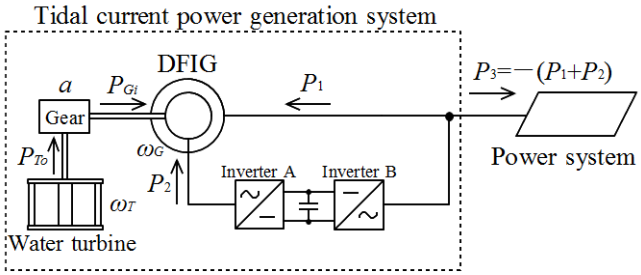

Fig. 8, Schematic illustration of tidal current power generation system.

the power output of the water turbine, ω_T is the angular speed of the water turbine, a is the gear ratio, P_{Gi} is the power supplied to the generator, ω_G is the angular speed of the generator, P_1 is the stator active power, and P_2 is the rotor active power. The power input to the generator is defined as positive for P_1 and P_2, while P_3 is defined as the power generated by the system, which consists of the DFIG and the inverter. Inverter B, which is attached to the rotor side, could also be used to compensate for reactive power, but in this study, the inputs and outputs were controlled to ensure it only supplied active power.

III. INVESTIGATION OF SPEED CONTROL MODEL

This section describes the construction of a speed control model capable of controlling the generator angular speed ω_G so that any desired water turbine output power P_{To} can be obtained for any current speed v.

3.1. WATER TURBINE OUTPUT POWER AND SLIP

The water turbine output power P_{To} at speed v is given by Eq. (20), and is the product of the water turbine input power P_{Ti} and the power coefficient C_P.

$$P_{To} = C_P P_{Ti} \tag{20}$$

The water turbine angular speed ω_T is given by Eq. (21), using the water turbine radius r and the tip speed ratio λ corresponding to the power coefficient C_P.

$$\omega_T = \frac{v\lambda}{r} \tag{21}$$

The generator angular speed ω_G is expressed using ω_T and the gear ratio a as:

$$\omega_G = a\omega_T \tag{22}$$

Using Eq. (22), the slip s can be written:

$$s = 1 - \frac{\omega_G}{\omega_s} = 1 - \frac{a\omega_T}{\omega_s} \tag{23}$$

where ω_s is the synchronous angular speed.

Using the water turbine output power P_{To} in Eq. (20) and the target slip s^* in Eq. (23) the stator current, rotor current and supply voltage for rotor can be calculated.

3.2. SUPPLY VOLTAGE FOR ROTOR

Using Eq. (24), the voltage equation for an induction generator can be expressed in rotating d-q coordinates [15]. Here, the q-axis is defined as lagging 90° behind the d-axis:

$$\begin{bmatrix} v_{ds} \\ v_{qs} \\ v_{dr} \\ v_{qr} \end{bmatrix} = \begin{bmatrix} r_1 + PL_{s1} & X_{s1} & PM & X_M \\ -X_{s1} & r_1 + PL_{s1} & -X_M & PM \\ PM & sX_M & r_2 + PL_{s2} & sX_{s2} \\ -sX_M & PM & -sX_{s2} & r_2 + PL_{s2} \end{bmatrix} \begin{bmatrix} i_{ds} \\ i_{qs} \\ i_{dr} \\ i_{qr} \end{bmatrix} \tag{24}$$

where v_{ds} and v_{qs} are the stator d and q axis voltages, i_{ds} and i_{qs} are the stator d and q axis currents, v_{dr} and v_{qr} are the rotor d and q axis voltages, i_{dr} and i_{qr} are the rotor d and q axis currents, r_1 and r_2 are the stator and rotor resistances, and L_{s1}, L_{s2} and M are the self-inductances of the stator and rotor, and the excitation inductance, respectively. X_{s1}, X_{s2} and X_M are the self-reactances of the stator and rotor, and the excitation reactance, respectively, P is d/dt, and s is slip. All the values for the rotor side in the equations were calculated using the values on the stator side.

Next, values of the stator phase voltages e_{a1}, e_{b1} and e_{c1} on the d-q axes are converted using:

$$\begin{bmatrix} v_{ds} \\ v_{qs} \end{bmatrix} = \sqrt{\frac{2}{3}} \begin{bmatrix} \cos\omega t & \cos(\omega t - 2\pi/3) & \cos(\omega t + 2\pi/3) \\ \sin\omega t & \sin(\omega t - 2\pi/3) & \sin(\omega t + 2\pi/3) \end{bmatrix} \begin{bmatrix} e_{a1} \\ e_{b1} \\ e_{c1} \end{bmatrix} \tag{25}$$

where ω is the frequency of the power source. If e_{a1}, e_{b1}, and e_{c1} are the rated voltages and are maintained, they are given by:

$$\left.\begin{aligned} e_{a1} &= \sqrt{2}E_s \sin\omega t \\ e_{b1} &= \sqrt{2}E_s \sin(\omega t - \frac{2}{3}\pi) \\ e_{c1} &= \sqrt{2}E_s \sin(\omega t + \frac{2}{3}\pi) \end{aligned}\right\} \tag{26}$$

where E_s is the root mean square value of the stator phase voltage.

When the stator voltages in Eq. (26) are substituted into the d-q axes conversion expression in Eq. (25), we obtain Eq. (27), providing the stator d and q axis voltages v_{ds}, and v_{qs}:

$$\left.\begin{aligned} v_{ds} &= 0 \\ v_{qs} &= \sqrt{3}E_s \end{aligned}\right\} \tag{27}$$

In order to reduce the required capacity of the rotor inverter, an excitation current is supplied from the stator. The target stator d-axis current is then given by:

$$i_{ds}^* = -\frac{\sqrt{3}E_s}{r_1^2 + X_{s1}^2} X_{s1} \tag{28}$$

If it is assumed that gear losses can be neglected with regard to the water turbine output power P_{To} and the generator input power P_{Gi}, using Fig. 8 we obtain:

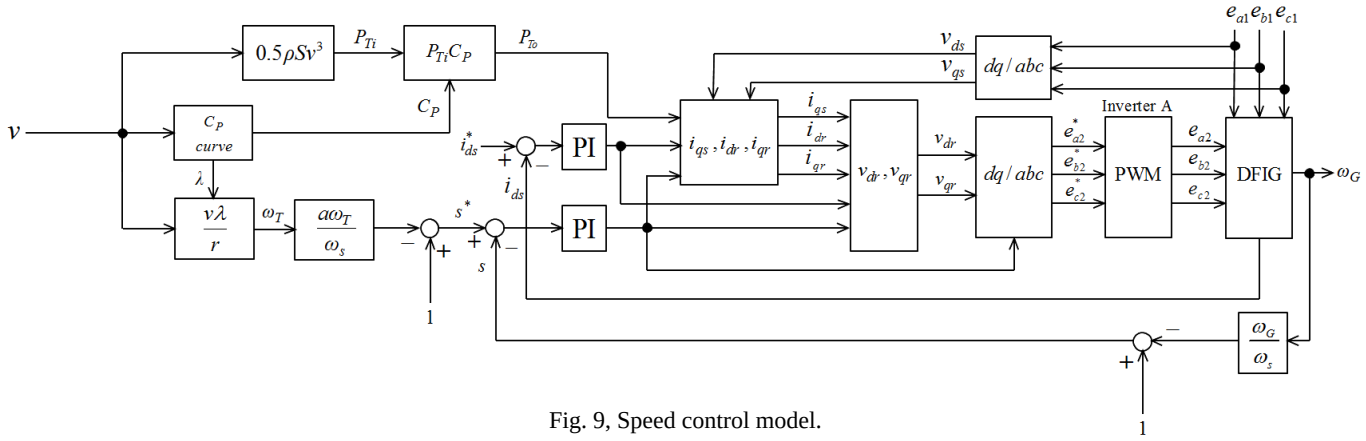

Fig. 9, Speed control model.

$$P_{To} = P_{Gi} = (1-s)X_M(i_{qs}i_{dr} - i_{ds}i_{qr}) \quad (29)$$

We find the stator and rotor currents i_{qs}, i_{dr}, i_{qr} from the target slip s^* in Eq. (23) and from the relations among the target stator d-axis current i_{ds}^* given by steady-state rows 1 and 2 in Eq. (24), and Eq. (28), the generator input power P_{Gi} in Eq. (29) and the water turbine output power P_{To}.

The d- and q-axes rotor voltages v_{dr} and v_{qr} are found using Eqs. (30) and (31), on the basis of rows 3 and 4 in Eq. (24).

$$v_{dr} = s^* X_M i_{qs} + r_2 i_{dr} + s^* X_{s2} i_{qr} \quad (30)$$

$$v_{qr} = -s^* X_M i_{ds}^* - s^* X_{s2} i_{dr} + r_2 i_{qr} \quad (31)$$

3.3. Equation of Motion

The generated torque T_e is obtained by dividing the generator input power P_{Gi} by the angular generator speed ω_G:

$$T_e = pM(i_{qs}i_{dr} - i_{ds}i_{qr}) \quad (32)$$

where p is the number of pole pairs of a DFIG.

The equation of motion is:

$$J\frac{d\omega_G}{dt} = T_T - T_e \quad (33)$$

where J is the total inertial moment of the turbine and the generator, and T_T is the turbine torque.

Figure 9 shows a schematic diagram of the complete speed control system model constructed in this study. As described above, the period of tidal fluctuations is long, so the compensation in this model is of the PI type.

IV. Investigation of Gear Ratio Maximizing Generated Energy

We now attempt to find a gear ratio and generator capacity that maximize the energy generated by the tidal current power generation system without overloading the generator during changes in the current speed while this system is operated under the above control schemes. Figure 10 shows the operating points of the MPPT control scheme and the constant turbine-output control scheme.

The MPPT system controls the system in order to maintain

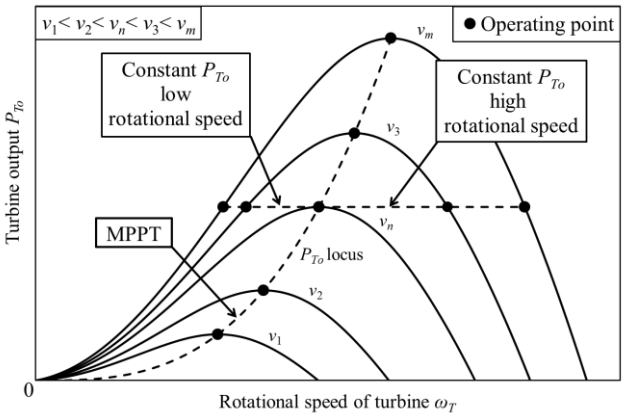

Fig. 10, Characteristics of turbine output.

the maximum possible water turbine power output up to the maximum current speed v_m, which gives the maximum annual energy production, as shown in Fig. 10. The constant turbine-output controller for the water turbine conducts MPPT at current speeds up to v (defined as the rated speed v_n) at which the stator current I_s or the rotor voltage E_r is at the rated value (1 pu), while at current speeds exceeding v_n, the operating point is controlled to hold the water turbine output constant. Constant turbine-output control can be performed in two ways: by maintaining the water turbine at a low speed with respect to v_n, the speed at which the water turbine output power would be maximized, or by maintaining it at a speed higher than v_n. If the turbine speed is kept low while the current speed exceeds v_n, there is a risk that I_s will exceed the rated value. However, if the turbine speed is kept high, there is a risk that E_r will exceed the rated value. Thus, when I_s or E_r exceed their rated values for any current speed below v_m, power generation is stopped, and that speed is subsequently

designated as v_{max}, the maximum current speed at which power can be generated.

This will be described in detail below, but an iterative technique must be employed in order to identify the gear ratio a and the rated capacity of the generator S_B that provide the maximum generated energy W. In this process, S_B changes with a, but the generator constants given by the per-unit method will not change within the range of variation in this investigation, so this method was used for calculating the generator parameters. To calculate the generated energy W during the observation time T using the probability density function for current speeds $f(v)$, we use:

$$W(a,S_B) = S_B T \int_{v_0}^{v_{max}} P_3(v) f(v) dv \tag{34}$$

Here, v_0 is the cut-in current speed [m/s].

4.1. MAXIMUM POWER POINT TRACKING CONTROL SCHEME

The values of a and S_B resulting in the maximum value for W in the MPPT scheme described in Eq. (34) are found by solving for $\partial W/\partial a = 0$, $\partial W/\partial S_B = 0$. However, there is a risk that the generator voltage or current could exceed their rated values at the identified a or S_B. The stator current I_s, rotor current I_r and rotor supply voltage E_r must be held within their rated values (within 1 pu). The conditions necessary in order to guarantee this are:

$$\left.\begin{aligned} h_1(a,S_B) &= I_s - 1 \le 0 \\ h_2(a,S_B) &= I_r - 1 \le 0 \\ h_3(a,S_B) &= E_r - 1 \le 0 \end{aligned}\right\} \tag{35}$$

Identification of the gear ratio a and generator capacity S_B to maximize the generated energy W can be handled as an optimization problem using Eq. (34) as the objective function and Eq. (35) as an inequality constraint. The method of Lagrange multipliers can be used for optimization problems with inequality constraints [16]. The slack variable l is introduced into the inequality constraint to transform it into the equality constraint:

$$\left.\begin{aligned} h_i + l_i &= 0 \\ l_i &\ge 0 \end{aligned}\right\} (i=1\sim3) \tag{36}$$

Next, using the penalty constant γ and the Lagrange multiplier ψ from the objective function in Eq. (34) and the equality constraint in Eq. (36), we obtain the modified penalty function:

$$Q(a,S_B,\boldsymbol{L},\boldsymbol{\psi}) = -W + \sum_{i=1}^{3} \psi_i (h_i + l_i) + \frac{1}{\gamma} \sum_{i=1}^{3} (h_i + l_i)^2 \tag{37}$$

in which $\boldsymbol{L} = [l_1, l_2, l_3]^T$, $\boldsymbol{\psi} = [\psi_1, \psi_2, \psi_3]^T$ and γ is a constant ($\gamma > 0$). The negative sign is placed on W in order to change this from a maximization to a minimization problem.

If we follow the calculation method for Lagrange multipliers, γ is fixed at a low constant value while $\boldsymbol{\psi}$ is set at an arbitrary value, and the a, S_B and $\boldsymbol{L}$ values yielding the minimum Q are found.

We begin by minimizing $\boldsymbol{L}$. Whenever l_i satisfies $\partial Q/\partial l_i = 0$, the non-positive elements of l_i (i.e. $l_i \le 0$) are set to 0. Positive elements of l_i are retained as they are and assumed to minimize Q. We then obtain:

$$l_i = -\left(h_i + \frac{\gamma \psi_i}{2} \right) \tag{38}$$

Substituting Eq. (38) into Eq. (37), Q becomes a function of only a, S_B, $\boldsymbol{\psi}$, and γ, and this simplifies to:

$$Q(a,S_B,\boldsymbol{\psi}) = -W + \frac{1}{\gamma} \sum_{i \notin I} \left(h_i + \frac{\gamma \psi_i}{2} \right)^2 - \frac{\gamma}{4} \sum_{i=1}^{3} (\psi_i)^2 \tag{39}$$

where $I = \{ i \mid l_i > 0 \}$. For a and S_B to minimize Q, the following equations must be satisfied.

$$\frac{\partial Q}{\partial a} = -\frac{\partial W}{\partial a} + \frac{2}{\gamma} \sum_{i \notin I} \left(h_i + \frac{\gamma \psi_i}{2} \right) \frac{\partial h_i}{\partial a} = 0 \tag{40}$$

$$\frac{\partial Q}{\partial S_B} = -\frac{\partial W}{\partial S_B} + \frac{2}{\gamma} \sum_{i \notin I} \left(h_i + \frac{\gamma \psi_i}{2} \right) \frac{\partial h_i}{\partial S_B} = 0 \tag{41}$$

Solving Eqs.(40) and (41) allows us to find the values for the gear ratio a and the generator capacity S_B that minimize Q. However, since these are coupled nonlinear equations, initial values are estimated for a and S_B, and iterative calculations are performed until the following condition is satisfied:

$$\sum_{i=1}^{3} (h_i + l_i)^2 + \left(\frac{\partial Q}{\partial a} \right)^2 + \left(\frac{\partial Q}{\partial S_B} \right)^2 \le \zeta \tag{42}$$

where ζ is a very small positive constant. If Eq. (42) is never satisfied, $\boldsymbol{\psi}$ is revised in accordance with the rules given in Eq. (43) and the calculations are resumed using Eq. (37).

$$\psi_i = \begin{cases} 0 & , i \in I \\ \psi_i + \dfrac{2h_i}{\gamma} & , i \notin I \end{cases} \tag{43}$$

4.2. CONSTANT TURBINE-OUTPUT CONTROL SCHEME

Just as in MPPT, under constant turbine-output control, the a and S_B values that maximize W are found using Eq. (34) by solving $\partial W/\partial a = 0$ and $\partial W/\partial S_B = 0$. However, the control scheme changes under constant turbine-output control when the current speed surpasses the rated speed v_n, as shown in Fig. 10, so there is a discontinuity in the solution surface for W. Therefore, a genetic algorithm is employed to solve the maximization problem where the slope is discontinuous. Figure 11 shows the calculation process using the genetic algorithm in this study.

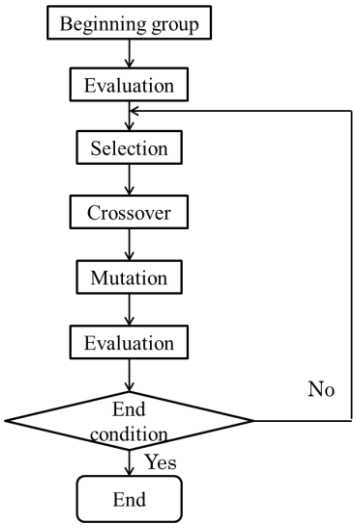

Fig. 11, Flow diagram for genetic algorithm.

4.3. Results of Calculations

Table 3 shows the parameters for the water turbine and DFIG obtained in the calculations to identify the gear ratio and generator capacity. The water turbine described in Table 3 is the model which the authors developed for use in an in-situ experiment, and is the largest we have ever tested [2]. Tables 4 and 5 present the results for the gear ratio and the generator capacity calculated for MPPT control and constant turbine-output control on the basis of the current speed data from 2003 and 2004. The annual capacity factor C_F shown in Tables 4 and 5 is defined as the ratio of the generated energy to that which would have been generated if the generator had operated for a full year at its full capacity. The energy conversion efficiency η_E is defined as the ratio of the annual generated energy to the annual tidal current energy passing through the swept area of the turbine S.

TABLE 3, Specifications and Constants for Tidal Current Power Generation

Water turbine	
Number of blades n	3
Height h [m]	1.6
Diameter d [m]	1.6
Chord length c [m]	0.3
Solidity σ	0.179
DFIG	
Rated voltage [V]	200
Number of pole pairs p	3
Frequency f [Hz]	50
Stator resistance r_1 [pu]	0.054
Rotor resistance r_2 [pu]	0.078
Stator leakage inductance L_{l1} [pu]	0.100
Rotor leakage inductance L_{l2} [pu]	0.100
Excitation inductance M [pu]	1.754

TABLE 4, Results for Gear Ratio and Rated Capacity of Generator (2003)

	MPPT	Constant P_{To}	
		High rotational speed	Low rotational speed
Gear ratio a	25.24	25.50	28.59
Rated capacity of generator S_B [kVA]	9.93	9.63	9.28
Rated capacity of inverter S_{BI} [kVA]	9.01	8.73	6.29
Annual generated energy W [MWh]	10.54	10.55	10.58
Energy conversion efficiency η_E [%]	21.15	21.17	21.24
Annual capacity factor C_F [%]	14.38	14.85	15.45
Cut-in current speed v_0 [m/s]	0.81	0.80	0.79
Generation maximum speed v_{max} [m/s]	3.90	3.86	3.90

TABLE 5, Results for Gear Ratio and Rated Capacity of Generator (2004)

	MPPT	Constant P_{To}	
		High rotational speed	Low rotational speed
Gear ratio a	25.50	25.77	29.10
Rated capacity of generator S_B [kVA]	9.63	9.33	8.89
Rated capacity of inverter S_{BI} [kVA]	8.73	8.47	5.97
Annual generated energy W [MWh]	10.53	10.53	10.57
Energy conversion efficiency η_E [%]	21.19	21.20	21.28
Annual capacity factor C_F [%]	14.77	15.25	16.08
Cut-in current speed v_0 [m/s]	0.80	0.79	0.78
Generation maximum speed v_{max} [m/s]	3.86	3.82	3.86

Tables 4 and 5 provide a comparison between constant turbine-output control and MPPT control on the basis of the 2003 and 2004 data; constant turbine-output control required a higher gear ratio but had a lower generator capacity. It also yielded a higher annual generated energy, annual capacity factor, and energy conversion efficiency.

The C_F under constant turbine-output control was 1.07% higher than that under MPPT control with the 2003 data, and 1.31% higher with the 2004 data.

V. Response of Speed Control Model

The response of the speed control model was examined using the values for a and S_B in the constant turbine-output control scheme for maximizing W in each year for the control schemes shown in Tables 4 and 5. The results are given in Fig. 9. The inputs were the estimated tidal current speed data for Akashi Strait published by the Japan Coast Guard Hydrographic and Oceanographic Department from January to December of 2003 and 2004 [14]. The highest current speed for each year (occurring on November 25, 2003 and June 3, 2004) was selected from the two data sets and used as v_m. These sets provided discrete values at 10-minute intervals, and these values were linearly interpolated.

Figure 12 shows a plot of v for 2003. The simulation results are provided in Figs. 13-18. The simulations were performed using MATLAB/Simulink in this study.

Figures 13 and 14 show the target values and the controlled values for the slip s and d-axis stator current i_{ds}. Good agreement is seen for both parameters, even for t = 2.7 to t = 4.5 h, when the turbine was under constant-output control,

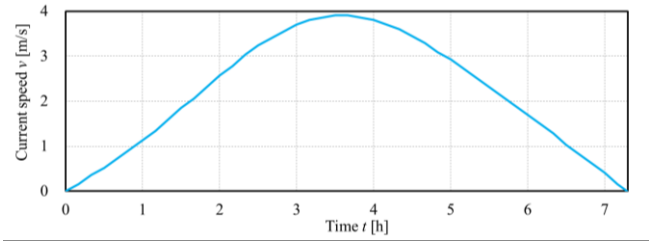

Fig. 12, Temporal change in current speed (2003).

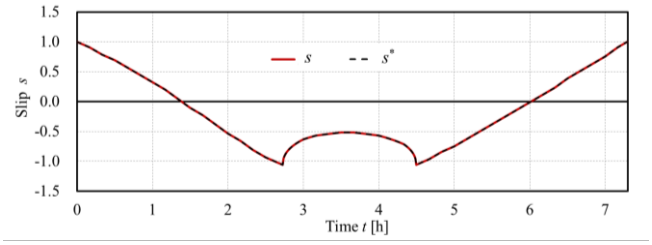

Fig. 13, Temporal change in slip (2003).

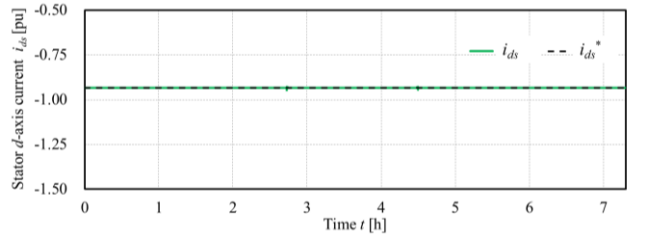

Fig. 14, Temporal change in stator d-axis current (2003).

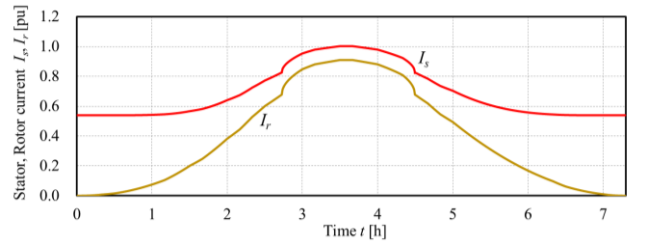

Fig. 15, Temporal change in stator and rotor currents (2003).

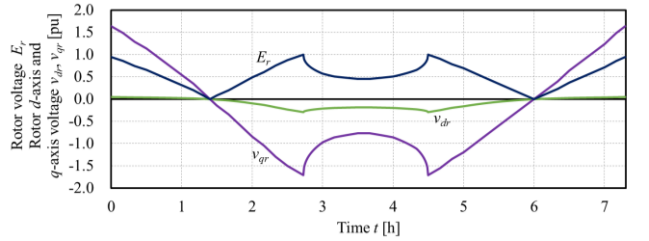

Fig. 16, Temporal change in rotor voltage, rotor d-axis voltage and rotor q-axis voltage (2003).

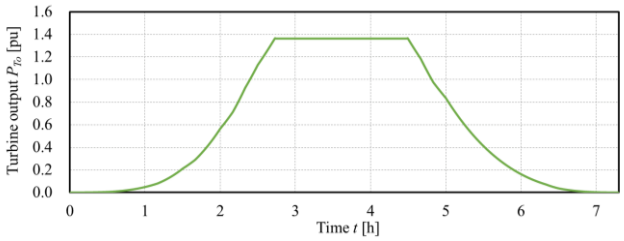

Fig. 17, Temporal change in turbine output (2003).

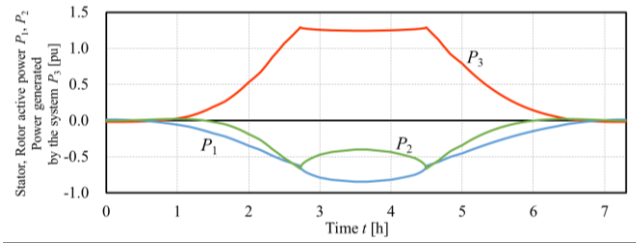

Fig.18, Temporal change in stator and rotor active power, power generated by the system (2003).

indicating a high degree of control. Figure 15 shows the stator and rotor currents I_s and I_r. As described above, I_s must supply excitation current from its d-axis current. Therefore, a current of 0.54 pu must always be flowing, and the stator current was held between 0.54 and 1.00 pu depending on the tidal current speed. The corresponding I_r values were between 0.00 and 0.91 pu. Figure 16 shows the d- and q-axes rotor voltages v_{dr} and v_{qr} and the rotor supply voltage E_r. v_{dr} varied between 0.05 and –0.30 pu and v_{qr} varied between 1.64 and –1.71 pu. E_r varied with current speed from 0.00 to 1.00 pu. Figure 17 shows P_{To} for the water turbine. P_{To} increased with current speed, and during constant turbine-output control, remained at a steady value of 1.37 pu. Figure 18 presents the stator and rotor active powers P_1 and P_2 and the power generated by the system P_3. P_1 was negative for nearly all current speeds, as it was supplying power to the power grid. P_2 was negative from t = 1.4 to 6.0 h; during this period, it was supplying power to the power grid through the inverter. P_3 increased with increasing current speed, reaching a maximum of 1.29 pu, and was approximately constant during constant turbine-output control. The value of P_3 with respect to P_{To}, i.e., the system efficiency η_s, for the current speed at which P_3 reached a maximum, was approximately 95%.

Turning to the 2004 data, Fig. 19 shows the temporal variation of v, and Figs. 20-25 show the simulation results.

Figures 20 and 21 show the slip s and the d-axis stator current i_{ds}, which both follow the target values well, even for t = 2.7 to 4.6 h during constant turbine-output control, indicating a high degree of control. Figure 22 presents the stator and rotor currents I_s and I_r. I_s varied between 0.54 and 1.00 pu depending on the current speed. Similarly, I_r varied from 0.00 pu to 0.91 pu. Figure 23 shows the d- and q-axes rotor voltages v_{dr} and v_{qr} and the rotor supply voltage E_r. As the current speed fluctuated, v_{dr} varied between 0.05 and –0.29 pu, v_{qr} varied between 1.64 and –1.71 pu, and E_r varied from 0.00 to 1.00 pu. Figure 24 shows the water turbine power output P_{To}; this parameter increased with current speed but was held constant at 1.35 pu during constant turbine-output

control. Figure 25 presents the stator and rotor active powers P_1 and P_2 and the power generated by the system P_3. P_1 was negative for nearly all current speeds, as it was supplying power to the power grid. P_2 was negative from t = 1.4 to 6.1 h; during this period, it was supplying power to the power grid through the inverter. P_3 increased with increasing current speed, reaching a maximum of 1.28 pu, and was approximately constant during constant turbine-output control. The value of P_3 with respect to P_{To} system efficiency η_s, was about 95% for the current speed at which P_3 reached a maximum.

In closing, the reason that P_3 exceeded the rated capacity of the generator using the inputs from 2003 and 2004 was that the generated power came not only from the stator, but also from the rotor via the inverter. This probably increased η_s. However, this investigation did not account for losses at the inverter and elsewhere, so η_s for an actual system would be expected to be lower.

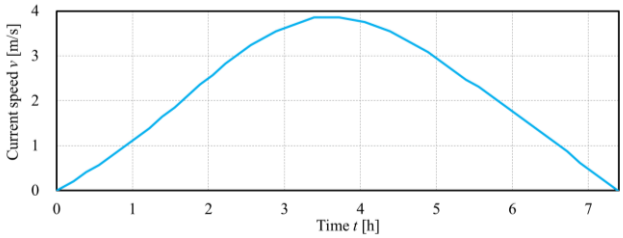

Fig. 19, Temporal change in current speed (2004).

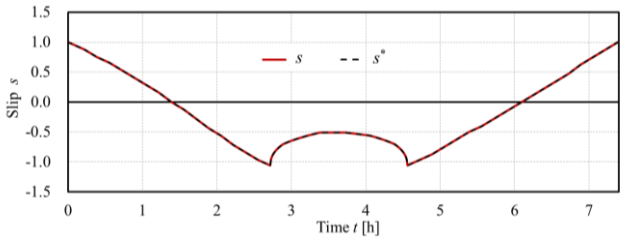

Fig. 20, Temporal change in slip (2004).

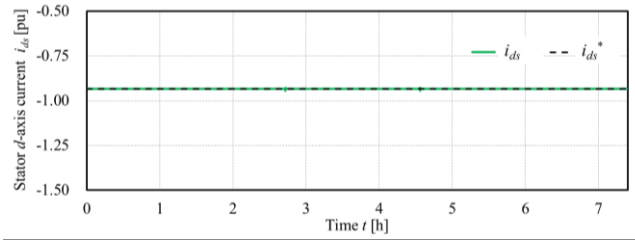

Fig. 21, Temporal change in stator *d*-axis current (2004).

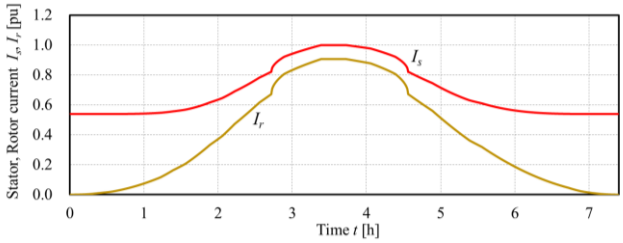

Fig. 22, Temporal change in stator and rotor currents (2004).

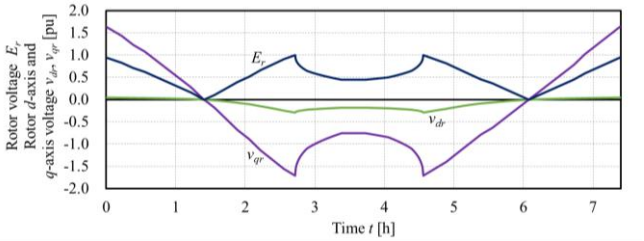

Fig. 23, Temporal change in rotor voltage, rotor *d*-axis voltage and rotor *q*-axis voltage (2004).

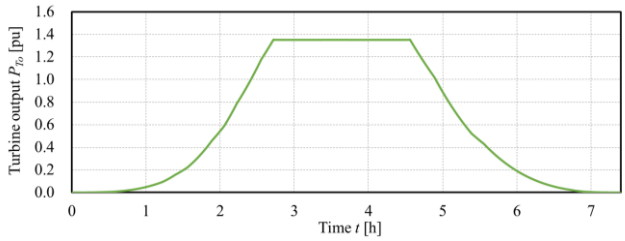

Fig. 24, Temporal change in turbine output (2004).

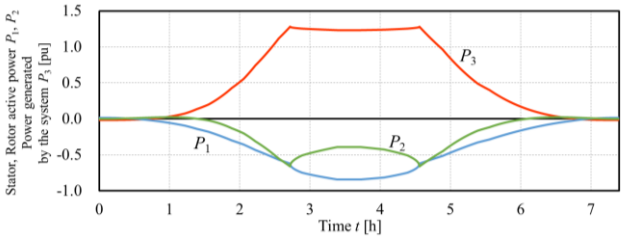

Fig. 25, Temporal change in stator and rotor active power, power generated by the system (2004).

VI. Conclusion

This study presented an investigation of a procedure for determining the gear ratio and the generator capacity for maximizing the generated energy without overloading a doubly-fed induction generator in a tidal current power generation system incorporating constant turbine-output control of the generator. A model was constructed for controlling the generator speed, while maintaining the water turbine at any desired speed during changes in current speed. The response of this model was examined with actual tidal current speed data. The following results were obtained in this study.

(1) The gear ratio and generator capacity resulting in the highest generated energy were calculated when a tidal current power generation system is operated under constant turbine-output control. This investigation indicated that constant turbine-output control results in higher electrical energy generation, allowing a generator with lower capacity, and a higher annual capacity factor of 16%, than a system operated under maximum power-point tracking.

(2) The response of a system operated under constant turbine-output control, with a gear ratio and generator capacity selected to generate the highest energy, was examined using actual varying tidal current speeds in a model of this controller. The target values for the slip and stator *d*-axis current were

followed well. The constant turbine-output control scheme was thus found to provide good control.

REFERENCES

[1] H. Kondo, H. Uehara, S. Kiho, T. Miyazaki, and K. Yano, *A Utilization Technology from Ocean Energy*, Tokyo: Morikita Publishing, 1996.

[2] S. Kihoh, M. Shiono, and K. Suzuki, "Power Generation from Tidal Currents," *International Symposium on Ocean Energy Development*, 1993, pp. 89-96.

[3] M. Shiono, K. Suzuki, and S. Kiho, "Experiments on the Characteristics of Darrieus Turbine for the Tidal Power Generation," *Proceedings of the Ninth International Offshore and Polar Engineering Conf.*, 1999, pp. 123-128.

[4] T. Ackermann, *Wind Power in Power Systems*, England: John Wiley & Sons, Ltd, 2005.

[5] R. Datta, and V. T. Ranganathan, "Variable-Speed Wind Power Generation Using Doubly Fed Wound Rotor Induction Machine - A Comparison With Alternative Schemes," *IEEE Trans. Energy Convers*., vol. 17, no. 3, pp. 414-421, Sep. 2002.

[6] M. Y. Uctug, I. Eskandarzadeh, and H. Ince, "Modeling and output power optimisation of a wind turbine driven double output induction generator," *IEE Proc.-Electr. Power Appl.*, vol. 141, no. 2, 1994, pp. 33-38.

[7] R. Datta, and V. T. Ranganathan, "Decoupled Control of Active and Reactive Power for a Grid-connected Doubly-fed Wound Rotor Induction Machine without Position Sensors," *Thirty-Fourth IAS Annual Meeting. Conference Record of the 1999 IEEE*, vol. 4, pp.2623-2630.

[8] A. Jain, and B. J. Reddy, "Control of Doubly Fed Induction Generator Connected to Variable Speed Wind Turbine," *2015 International Conference on Technological Advancements in Power and Energy*, pp. 500-505.

[9] A. Basak, K. Mukherjee, and P. Syam, "Speed Control of A Grid Connected Doubly-Fed Induction Generator System for Maximum Power Point Tracking with Improved Input Power Factor Employing Matrix Converter as a Slip Power Exchanger," *2016 IEEE First International Conference on Control, Measurement and Instrumentation*, pp. 42-47.

[10] K. Tsuji, K. Naoi, M. Shiono, and K. Suzuki, "Study on the Gear Ratio for a Tidal Current Power Generation System Using the MPPT Control Method," *Proceedings of the Twenty-fourth International Ocean and Polar Engineering Conf*., 2014, pp.568-574.

[11] Minister of Economy, Trade and Industry. Agency for Natural Resources and Energy. (2010) *Japan's energy 2010*. Available: http://www.enecho.meti.go.jp/about/pamphlet/energy2010html/policy/

[12] Ira H. Abbott, Albert E. Von Doenhoff, *Theory of wing sections*, New York: Dover Publications, Inc., 1959, p.339.

[13] K. Yoshimura, and F. Takayama. *The spline function by personal computer*, Tokyo: Tokyo Denki University Press, 1988.

[14] Japan Coast Guard, Hydrographic and Oceanographic Department. (2003, 2004) *Tide, tidal current information*. Available: http://www6.kaiho.mlit.go.jp/osakawan/index.htm

[15] D. W. Novotny, and T. A. Lipo, *Vector Control and Dynamics of AC Drives*, England: Oxford University Press, 1996.

[16] K. Shimizu, *System Optimization Theory*, Tokyo: CORONA Publishing Co., Ltd, 1976.